NASA TN D-3290

EFFECTS OF LEADING-EDGE BLUNTNESS AND RAMP DEFLECTION ANGLE ON LAMINAR BOUNDARY-LAYER SEPARATION IN HYPERSONIC FLOW

By James C. Townsend

Langley Research Center
Langley Station, Hampton, Va.

NATIONAL AERONAUTICS AND SPACE ADMINISTRATION

For sale by the Clearinghouse for Federal Scientific and Technical Information
Springfield, Virginia 22151 – Price $1.00

EFFECTS OF LEADING-EDGE BLUNTNESS AND RAMP DEFLECTION ANGLE ON LAMINAR BOUNDARY-LAYER SEPARATION IN HYPERSONIC FLOW

By James C. Townsend
Langley Research Center

SUMMARY

16589

An investigation to determine the effects of leading-edge bluntness on the characteristics of laminar boundary-layer separation induced on a flat plate by a trailing-edge ramp has been conducted in the Langley 15-inch hypersonic flow apparatus. Three leading-edge radii and five ramp deflection angles (0° to 40°) were tested on the plate at a Mach number of 10.03 and nominal Reynolds numbers of 1.26×10^5 and 1.56×10^5 per inch (4.96×10^6 and 6.14×10^6 per meter). All tests were made at zero angle of attack, and end plates were used to approximate two-dimensional flow conditions.

The results of the investigation indicate that at a Mach number of 10.03 there are considerable effects of leading-edge bluntness on the flow-separation characteristics. The pressure rise through the interaction region to the pressure plateau is much less and the extent of the separation region is much smaller with the 0.102-inch (0.258-cm) nose radius than with the sharp nose radius (radius less than 0.001 inch (0.003 cm)) for each ramp deflection angle. The pressure rise and the length of the separated-flow region are reduced by more than one-third for the higher ramp angles. A further increase in the nose radius to 0.203 inch (0.517 cm), however, produces only small additional changes in the pressure distribution and in the extent of the separation region. A comparison of the plateau pressure-rise coefficients with data from studies on sharp-nose plates indicates that the boundary-layer momentum thickness and the local Mach number and Reynolds number at the beginning of the interaction form the proper basis for comparison of boundary-layer separation characteristics on blunt- and sharp-nose configurations.

Author

INTRODUCTION

An understanding of flow-separation phenomena is of great importance in the design of aircraft because the difference between the actual surface pressure distribution in a region where the flow is separated from the surface and the distribution predicted theoretically for flow following the surface contour may be very large. A large difference in these distributions could result in an appreciable alteration of the aerodynamic forces and moments acting on an aircraft or its components.

Shock waves, such as those generated by deflected control surfaces in supersonic flows, frequently impose a sufficiently strong pressure gradient on the boundary-layer flow to cause flow separation ahead of the shock. At hypersonic speeds, the effects of such separation are especially pronounced because of the large pressure ratio across the strong shock waves generated by even small flow deflections.

Several experimental studies of flow separation involving laminar boundary layers have been made at supersonic and hypersonic speeds. (See, for example, refs. 1 to 4.) The flow separation studied has generally been that occurring when the laminar boundary layer on a sharp-edge plate interacts with a shock wave generated either by an external source or by a ramp or forward-facing step on the plate surface. These studies for sharp-edge plates have shown that the strength of this imposed shock wave and also the local Mach number and Reynolds number at the beginning of the interaction (i.e., where the basic surface pressure distribution is first increased by the flow separation) are the important parameters that affect the extent of the region of separated flow and the associated surface pressure distribution. Most designs for hypersonic aircraft, however, require some degree of bluntness on wing leading edges in order to avoid structural and heating difficulties. The fact that leading-edge bluntness has a strong effect on the local flow parameters near the wing surface for a considerable distance behind the leading edge indicates that bluntness will strongly affect any flow separation which occurs.

Therefore, the present investigation was undertaken to determine the nature of the effects of leading-edge bluntness on shock-induced two-dimensional laminar flow separation at hypersonic speeds. Surface pressure distributions were obtained on a flat-plate model with variable degrees of leading-edge bluntness; trailing-edge ramps of various deflection angles were used to generate flow separation. Plate leading-edge radii ranged from approximately 0 to 0.203 inch (0.517 cm) and ramps provided deflection angles from 0° to 40°. The test Mach number was 10.03, and most of the tests were made at a nominal free-stream Reynolds number of 1.26×10^5 per inch (4.96×10^6 per meter). End plates were used on the model to approximate two-dimensional flow conditions in the central region of the plate where the pressure distributions were measured.

SYMBOLS

The units used for the physical quantities defined in this paper are given both in the U.S. Customary Units and in the International System of Units (SI). Factors relating the two systems are given in reference 5.

$C_{p,p}$ plateau pressure coefficient, $\frac{p_p - p_o}{q_o}$

c_f local skin-friction coefficient

K empirical constant in plateau pressure correlation

L total model length, 10 inches (25.4 centimeters)

l length of flat surface ahead of ramp leading edge, 8.725 inches (22.16 centimeters)

M Mach number

p static pressure

p_o' static pressure at point on basic plate ($\theta = 0^o$) corresponding to the beginning of interaction on plate with ramp deflection

q dynamic pressure

R_∞ Reynolds number based on free-stream conditions, $\frac{\rho_\infty V_\infty x}{\mu_\infty}$

$R_{x,o}$ Reynolds number based on test conditions at beginning of interaction, $\frac{\rho_o V_o x_o}{\mu_o}$

$R_{\bar{x},o}$ Reynolds number based on $\bar{x}_o$ and test conditions at beginning of interaction, $\frac{\rho_o V_o \bar{x}_o}{\mu_o}$

r plate leading-edge radius

T temperature

V velocity

x longitudinal coordinate, origin at beginning of flat surface of plate (see fig. 1)

$\bar{x}$ length of sharp-leading-edge plate necessary to attain momentum thickness equal to that at coordinate x on blunted plate

$\beta = \sqrt{|M^2 - 1|}$

θ ramp deflection angle

μ coefficient of viscosity

ρ mass density of air

Subscripts:

o conditions at beginning of interaction

p conditions in pressure-plateau region

t stagnation conditions

∞ free-stream conditions

MODEL

The basic model consisted of an 8- by 10-inch (25.4- by 20.3-cm) stainless-steel flat plate mounted on a swept strut projecting from the test-section floor. Five ramps were provided for attachment at the rear of the plate (fig. 1); the ramps had deflection angles of 0°, 10°, 20°, 30°, and 40°, and

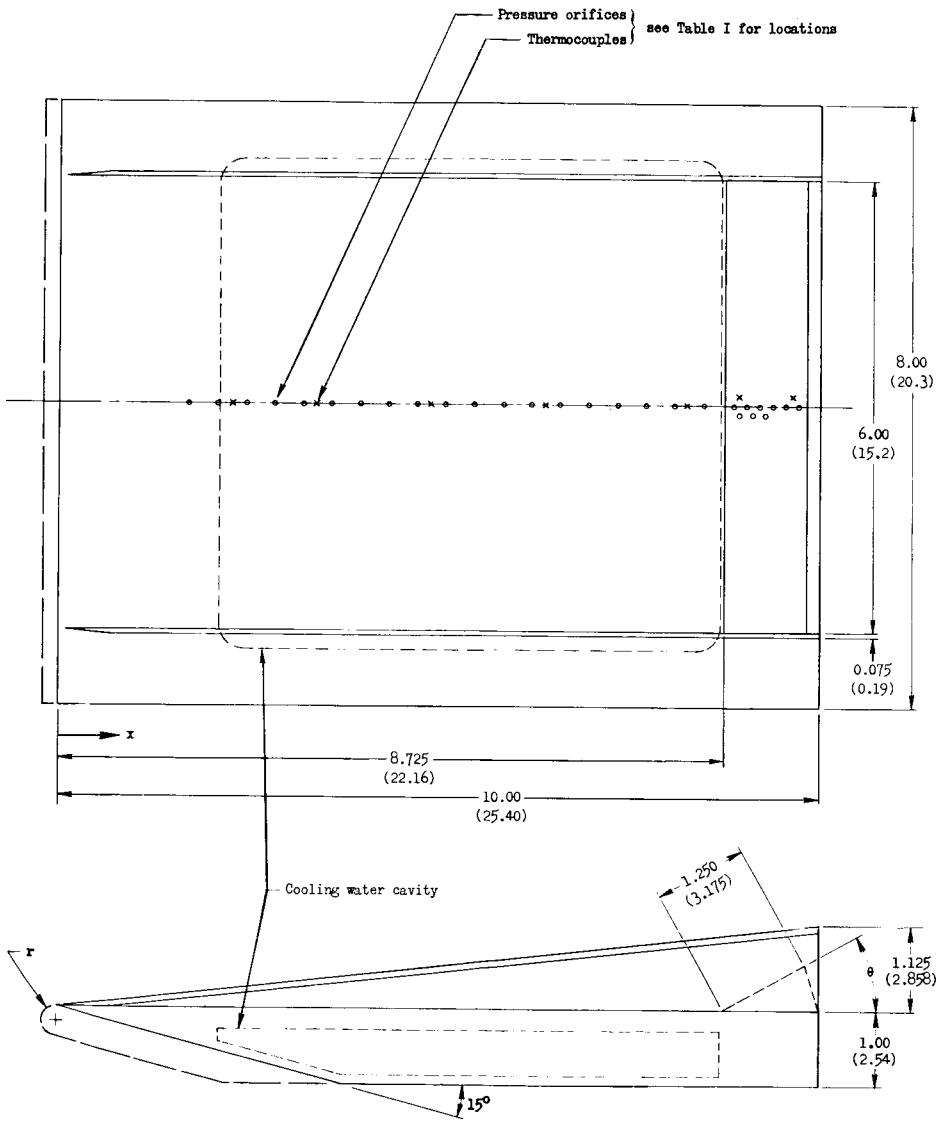

Figure 1.- Drawing of model. All linear dimensions are given first in inches and parenthetically in centimeters.

each had a chord of 1.25 inches (3.18 cm) and a span of 6 inches (15.2 cm). In addition to the sharp nose radius of the basic plate ($r < 0.001$ inch (0.003 cm)), two interchangeable hemicylindrical noses with radii of 0.102 and 0.203 inch (0.258 and 0.517 cm) were provided for varying the degree of nose bluntness. (See figs. 1 and 2.) End plates were used to produce two-dimensional flow conditions over the central region of the model surface.

Nineteen orifices for surface pressure measurements were located along the center line of the plate. Nine additional orifices were located on each of the ramps; however, the pressure-distribution data for the ramps are not presented because difficulties arose in obtaining reliable pressure measurements with the type of gage used with the ramp orifices. Thermocouples for surface temperature measurements were embedded at five locations on the plate and two locations on each ramp. The locations of the plate orifices and the thermocouples are given in table I.

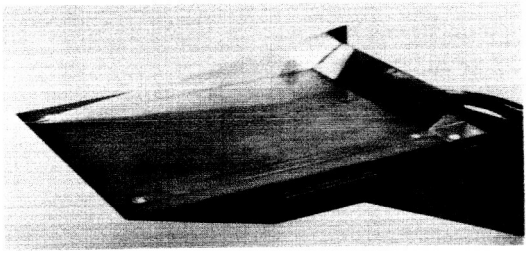

(a) $r < 0.001$ in. (0.003 cm); $\theta = 30^\circ$ (near end plate removed).

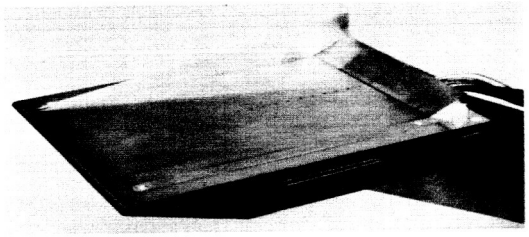

(b) $r = 0.102$ in. (0.258 cm); $\theta = 20^\circ$ (near end plate removed).

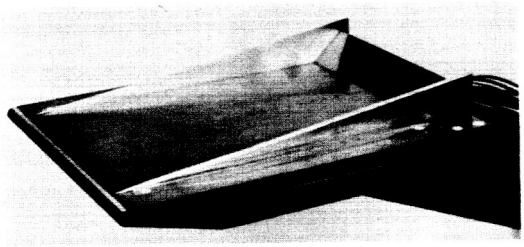

L-65-9033

(c) $r = 0.203$ in. (0.517 cm); $\theta = 40^\circ$ (both end plates in place).

Figure 2.- Photographs of three model configurations.

TABLE I.- LOCATIONS OF ORIFICES AND THERMOCOUPLES ON MODEL[1]

Pressure orifices					
Identity number	Distance from sharp leading edge		Identity number	Distance from sharp leading edge	
	in.	cm		in.	cm
1	1.712	4.348	11	5.465	13.881
2	2.096	5.324	12	5.845	14.846
3	2.468	6.269	13	6.213	15.781
4	2.840	7.214	14	6.587	16.731
5	3.216	8.169	15	6.966	17.694
6	3.593	9.126	16	7.340	18.644
7	3.968	10.078	17	7.716	19.599
8	4.340	11.024	18	8.087	20.541
9	4.714	11.974	19	8.466	21.504
10	5.091	12.931			
Thermocouples					
Identity number	Distance from sharp leading edge		Identity number	Distance from ramp hinge line	
	in.	cm		in.	cm
1	2.28	5.79	6	0.22	0.56
2	3.39	8.61	7	1.02	2.59
3	4.90	12.45			
4	6.40	16.26			
5	8.25	20.96			

[1]All pressure orifices and thermocouples are located within 0.01 inch (0.03 cm) of the center line. Ramp thermocouples are 0.125 inch (0.3 cm) from the center line.

APPARATUS AND TESTS

The tests were conducted in the Langley 15-inch hypersonic flow apparatus, a blowdown facility with running times of up to $2\frac{1}{2}$ minutes. The flow is very nearly uniform at a Mach number of 10.03 throughout a central region approximately 10 inches (25.4 cm) in diameter and at least 16 inches (41 cm) long at the test-section window (ref. 6).

Surface pressures on the plate were measured with heat-conduction type gages having a sensitive range from 0.01 to 0.10 psia (0.07 to 0.70 kN/m^2). These gages were all simultaneously calibrated with the reference pressures in both ascending and descending order so that possible hysteresis effects could be determined. Model surface temperatures were measured with chromel-alumel thermocouples embedded in the model surface; the reference junction was maintained at 150° F (339° K). All data were recorded on strip charts with pens positioned by self-balancing potentiometers.

The pressure gages for measuring the plate pressure distributions were mounted outside the tunnel and connected to the 0.060-inch-diameter (1.5-mm) orifices by means of 0.090-inch (2.3-mm) inside-diameter stainless-steel tubing. The length of the tubing was kept as short as possible (less than $2\frac{1}{2}$ feet (0.76 m)) to minimize the pressure lag times. An approximately constant surface temperature was maintained by circulating cooling water through the strut into an internal cavity of the model (fig. 1). Circulating water through the model also kept the temperature uniform for all test runs.

The principal series of tests was made at a nominal stagnation pressure of 815 psia (5.62 MN/m^2) and a stagnation temperature of 1100° F (866° K); the corresponding free-stream Reynolds number was 1.26×10^5 per inch (4.96×10^6 per meter). In order to investigate the effects of increasing the Reynolds number to about 1.56×10^5 per inch (6.14×10^6 per meter), three additional runs were made with $p_t \approx 1015$ psia (7.00 MN/m^2) and $T_t \approx 1130°$ F (883° K). Table II lists the configurations and the corresponding free-stream unit Reynolds numbers for the present investigation. No test data were obtained for the configuration with the plate leading-edge radius less than 0.001 inch (0.003 cm) and the ramp deflection angle of 40° because of the blockage of this configuration, which prevented the tunnel from starting. Although blunt-nose configurations presumably would impose more tunnel blockage than sharp-nose configurations, the addition of nose bluntness in the present investigation, in fact, reduced the strength of the shock wave ahead of the 40° ramp sufficiently to reduce the total blockage and allow the tunnel to start.

It should be noted that the stagnation temperatures used in the present investigation are below those theoretically required to avoid air condensation; however, the results of references 7 and 8 have shown that sufficient supersaturation occurs in Mach 10 wind tunnels to prevent liquefaction for stagnation temperatures at least 100° F or 56° K below those actually used for the present

tests. Independent experiments reported in reference 9 confirm the validity of these results for the hypersonic flow apparatus used in the present investigation.

TABLE II.- CONFIGURATIONS TESTED IN PRESENT INVESTIGATION

(a) U.S. Customary Units

Leading-edge radius, in.	End plates	Free-stream Reynolds number per inch for ramp deflection angle of -				
		0°	10°	20°	30°	40°
0.001	On	1.27×10^5	1.26×10^5 1.54	1.24×10^5	1.26×10^5	
.001	Off	1.28	1.30	1.25	1.18	
.102	On	1.26 1.58	1.27	1.22	1.28 1.56	1.23×10^5
.102	Off				1.27	
.203	On	1.25	1.26	1.23	1.31	1.29
.203	Off	1.26	1.28		1.26	

(b) International System of Units

Leading-edge radius, cm	End plates	Free-stream Reynolds number per meter for ramp deflection angle of -				
		0°	10°	20°	30°	40°
0.003	On	5.00×10^6	4.96×10^6 6.06	4.88×10^6	4.96×10^6	
.003	Off	5.04	5.12	4.92	4.65	
.258	On	4.96 6.22	5.00	4.80	5.04 6.14	4.84×10^6
.258	Off				5.00	
.517	On	4.92	4.96	4.84	5.16	5.08
.517	Off	4.96	5.04		4.96	

The wall temperatures of the plate and ramps varied somewhat for the different runs, primarily because of the effects of flow separation on heat transfer to the surface. The range of the ratio of wall temperature to free-stream static temperature for the present test series is shown in figure 3. No attempt was made to extract heat-transfer information from the wall temperature measurements.

It was expected that the low-speed flow in the region of flow separation on the plate would be sensitive to any lateral pressure gradients which might exist because of edge effects of the finite-span ramps. For this reason, end plates were used on the model in the principal series of tests to ensure essentially two-dimensional flow conditions. Some additional runs were made without end plates so that comparison data could be obtained and schlieren photographs could be taken. In figure 4 the pressure distributions are shown for some typical configurations with and without end plates. As can be seen, removing the end plates has no effect on the basic pressure distributions either on the plates with no separation or on the surface areas ahead of the separated-flow regions. However, removal of the end plates in the separated-flow regions causes a reduction of the pressure distributions. These results indicate that there is no significant interaction of the end plates with the flat-plate boundary layer, and that the lowering of the pressure distributions in the separated-flow region when the end plates are removed is due to the outflow of air around the ends of the ramps.

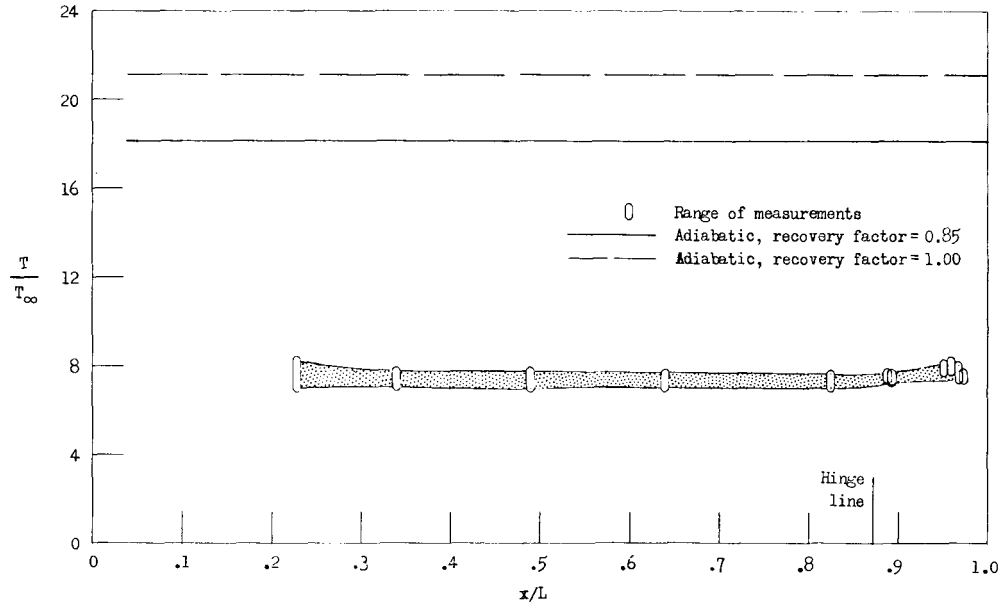

Figure 3.- Range of ratio of wall to free-stream temperature for complete test series.

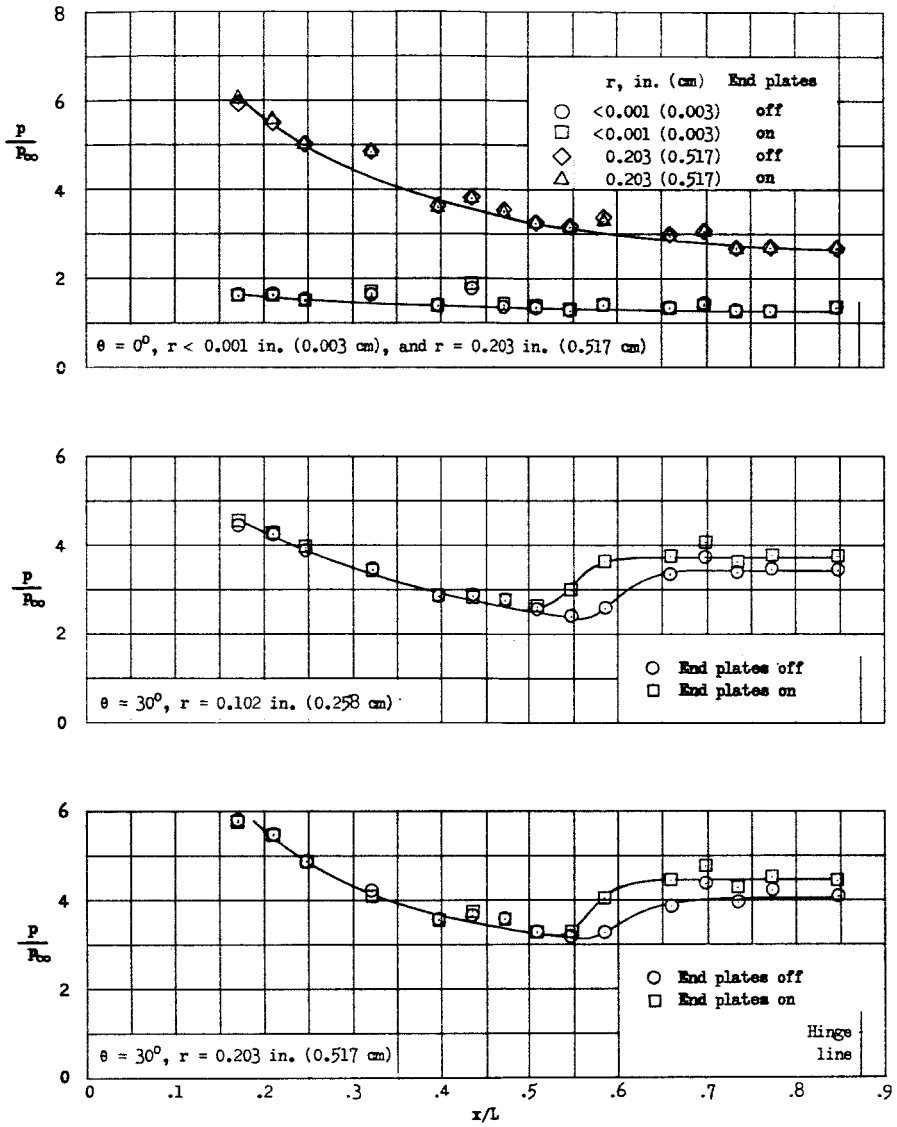

Figure 4.- Effect of use of end plates on the pressure distribution for several configurations.

In order to accommodate the outputs from the thermocouples and pressure gages to the available strip-chart recorders, the pressure gages were divided into three groups of 9 or 10 gages each. All the pressure data were obtained on 10 recorders by recording data from the gages of each group simultaneously and switching electrically among the groups during the run. The procedure followed in testing was to start the tunnel with the switch in the first position and then to wait at least 45 seconds to allow for the lag in the pressure tubing; the rest of the cycle through the other two switch positions was completed in approximately 15 seconds. The switch was returned to the first position so that a check on any change which might have occurred during the cycling time could be made. (Trials before the testing had shown that the pressure

tubing had lag times on the order of 30 seconds.) The stagnation conditions and model surface temperatures were recorded continuously throughout each run.

ACCURACY OF DATA

The manufacturer's quoted accuracy of the gages used to measure the plate surface pressures is 1 percent of the range of 20 millimeters of mercury (2.7 kN/m^2), or about 0.004 psia (0.03 kN/m^2), based on point repeatability. The calibration procedure used is considered to be sufficiently accurate to produce no additional significant errors.

At the low pressure levels involved in the present studies, considerable difficulty was experienced in eliminating outgassing and vacuum leakage in the joints and tubing which led from the orifices to the gages. Despite considerable efforts to reduce all leakage, a sufficient amount remained to make the data at four orifices useless and to cause small increases in the pressures measured at several others. These apparent increases have been accounted for in fairing the curves of the plotted data.

RESULTS AND DISCUSSION

Presentation of Results

The effects of ramp-angle variation on the flow over the sharp-nose flat plate are shown in the schlieren photographs of figure 5 and in the center-line surface pressure distributions of figure 6. The effects of nose bluntness are shown in the schlieren photographs of figure 7 and the surface pressure distributions of figure 8. In figure 9 is presented the effect of leading-edge bluntness on the magnitude of the ratio $\frac{p - p_o}{p_\infty}$, which represents the increment in pressure above the level at the beginning of the interaction (i.e., where the pressure distribution is first increased by the flow separation). These data are also presented in figure 10 with the basic pressure distribution ($\theta = 0^\circ$) subtracted in order to show the total difference between the pressure distribution resulting from flow separation and the distribution that would exist in the absence of separation (i.e., if the basic flat-plate pressure distribution continued up to the ramp hinge line). The effects of leading-edge bluntness and ramp deflection angle on the characteristics of the separated-flow region are summarized in figure 11; the local Mach number and Reynolds number at the beginning of the interaction are also plotted in this figure. In figure 12, the pressure distributions for the flat plate with no ramp deflection are compared with theory for three leading-edge radii. Figure 13 presents the results of correlations of the data obtained in the present investigation with results from other sources.

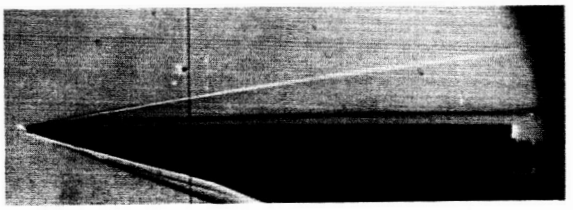

(a) $\theta = 0^{\circ}$.

(b) $\theta = 10^{\circ}$.

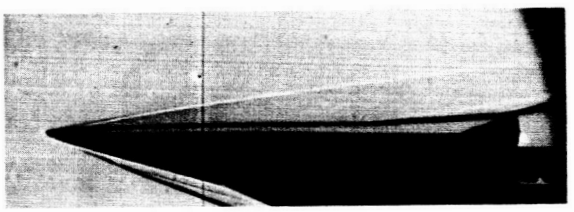

(c) $\theta = 20^{\circ}$.

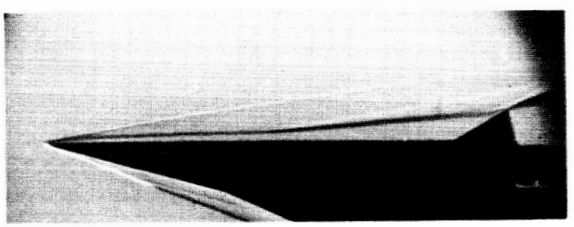

(d) $\theta = 30^{\circ}$. L-65-9034

Figure 5.- Schlieren photographs showing the effect of varying ramp deflection angle on the flow over a flat plate with a sharp leading edge. $R_{\infty}/x = 1.26 \times 10^{5}$ per inch $(4.96 \times 10^{6}$ per meter); $r < 0.001$ inch (0.003 cm); end plates off.

Experimental Results

Effect of ramp angle.- The schlieren photographs of figure 5 show the changes in the flow pattern for the sharp-leading-edge plate as the ramp angle is varied from 0° to 30°. Above the plate surface are light lines indicating shock waves and a dark line indicating the density gradient at the edge of the thermal boundary layer. Inasmuch as the thermal and velocity boundary layers very nearly coincide for laminar flow at hypersonic speeds, the dark line also indicates the approximate edge of the velocity boundary layer. The flow-separation region appears in the photographs as the part of the boundary layer ahead of the ramp downstream of the point where the angle relative to the plate of the boundary-layer edge (dark line) suddenly changes. As the angle of the ramp with constant length is increased, the beginning of the separated-flow region moves forward on the plate. The corresponding movement of the sharp pressure rise which precedes the almost constant level or "plateau" pressure, which is characteristic of flow separation, can be seen in figure 6. This plateau pressure, which occurs for all nose bluntnesses, increases with increased ramp deflection angle while the separation point simultaneously moves forward on the plate. As a result, an increasing percentage of the plate area is exposed to an increasing amount of pressure as the ramp deflection angle increases. This effect may be seen clearly in the summary plots of figure 11.

Effect of nose bluntness.- The effect on the flow pattern of increasing the leading-edge radius is shown in the schlieren photographs of figure 7 for the 30° ramp. Unfortunately, the boundary-layer edge is not visible for the blunt-nose plates because the very low density of the flow near the body decreases the sensitivity of the schlieren system and because the highly curved shock wave produces strong density

gradients throughout the entire nonuniform flow region that tend to obscure the density gradient at the boundary-layer edge. However, increasing the bluntness moves the shock wave originating at the separation point rearward; this movement indicates that increased bluntness results in an appreciable reduction in the extent of the separated region.

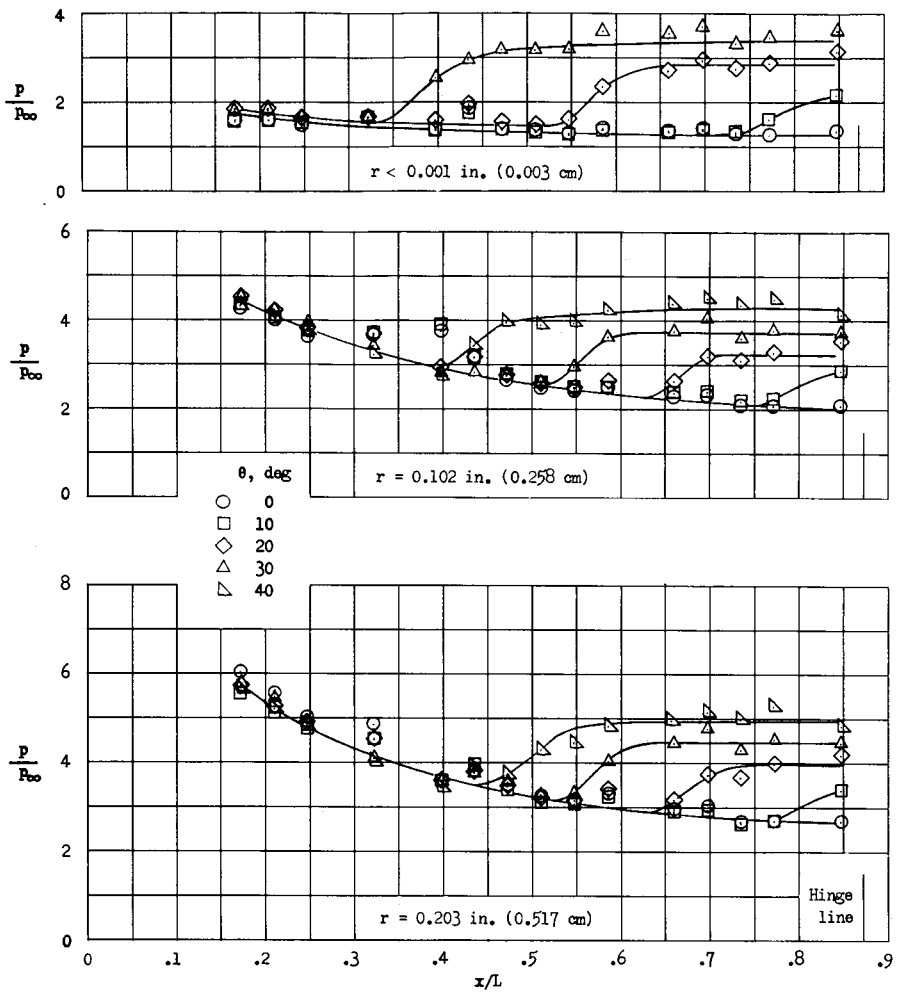

Figure 6.- Effect of ramp deflection angle on the flat-plate pressure distribution for the three leading-edge radii. End plates on; $R_\infty/x = 1.26 \times 10^5$ per inch $(4.96 \times 10^6$ per meter).

The reduced lengths of the separated regions are evident in the pressure distributions of figure 8. In this figure, however, the effects of the bluntness on the magnitude of the separated-flow pressure rise are somewhat obscured by the more fundamental effect of increased basic flat-plate pressure distributions. Figures 9 and 10, which include the same data brought to a common basis for comparison, show that the pressure rise from the beginning of the interaction to the pressure plateau and the length of separation are considerably reduced by increasing the nose radius from less than 0.001 to 0.102 inch (from $r < 0.003$ to $r = 0.258$ cm). Increasing the nose radius from 0.102 to 0.203 inch

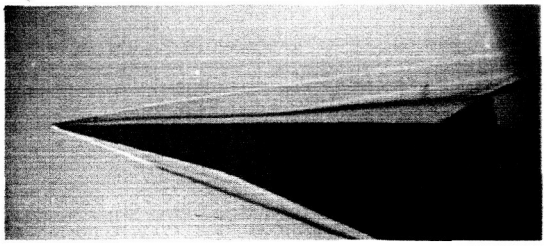

(a) $r < 0.001$ in. (0.003 cm).

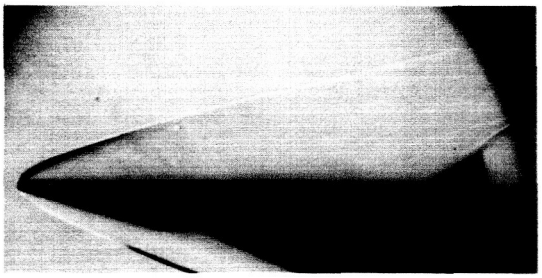

(b) $r = 0.102$ in. (0.258 cm).

L-65-9035

(c) $r = 0.203$ in. (0.517 cm).

Figure 7.- Schlieren photographs showing the effect of varying the leading-edge radius on the flow over a flat plate with a 30° ramp. $R_\infty/x = 1.26 \times 10^5$ per inch (4.96×10^6 per meter); end plates off.

(0.258 to 0.517 cm), however, produces only a small further reduction in the separation length and practically no further reduction in the pressure rise to the plateau. These results clearly show that, within the test ranges, leading-edge bluntness produces a favorable moderation of the effects of laminar boundary-layer separation due to pressure rises associated with components such as air inlets and deflected controls.

It is expected that these moderating effects of leading-edge bluntness on the characteristics of the separated-flow region are associated with the large bluntness-induced changes in the flow properties on the plate. In order to examine this relationship, the local Mach number and Reynolds number at the beginning of the interaction leading to separation were calculated by assuming for the two blunt-leading-edge plates that the flow at the edge of the boundary layer had passed through a nearly normal segment of the shock wave generated by the blunt nose and that the stagnation pressure was constant along the boundary-layer edge. The normal shock relations for the free-stream Mach number (10.03) and stagnation pressure were used to find the stagnation pressure behind the shock, which, according to the above assumption, is also the local stagnation pressure just outside the boundary layer. The ratio of the measured local static pressure to this local stagnation pressure was used in the isentropic flow relations to obtain the local Mach number at the edge of the boundary layer. For the sharp-nose plate, the oblique-shock relations were used to determine the local stagnation pressure; a 12° leading-edge shock angle (measured from the schlieren photographs) was used in this calculation. The local Mach number was then found as previously. The local Reynolds number for each test was found by using the local Mach number and stagnation pressure, the stagnation temperature, and the length along the plate to the beginning of the interaction. As may be seen in figure 11, both M_o and $R_{x,o}$ decrease rapidly with increasing leading-edge radius and become nearly constant for leading-edge radii greater than about 0.1 inch (0.3 cm).

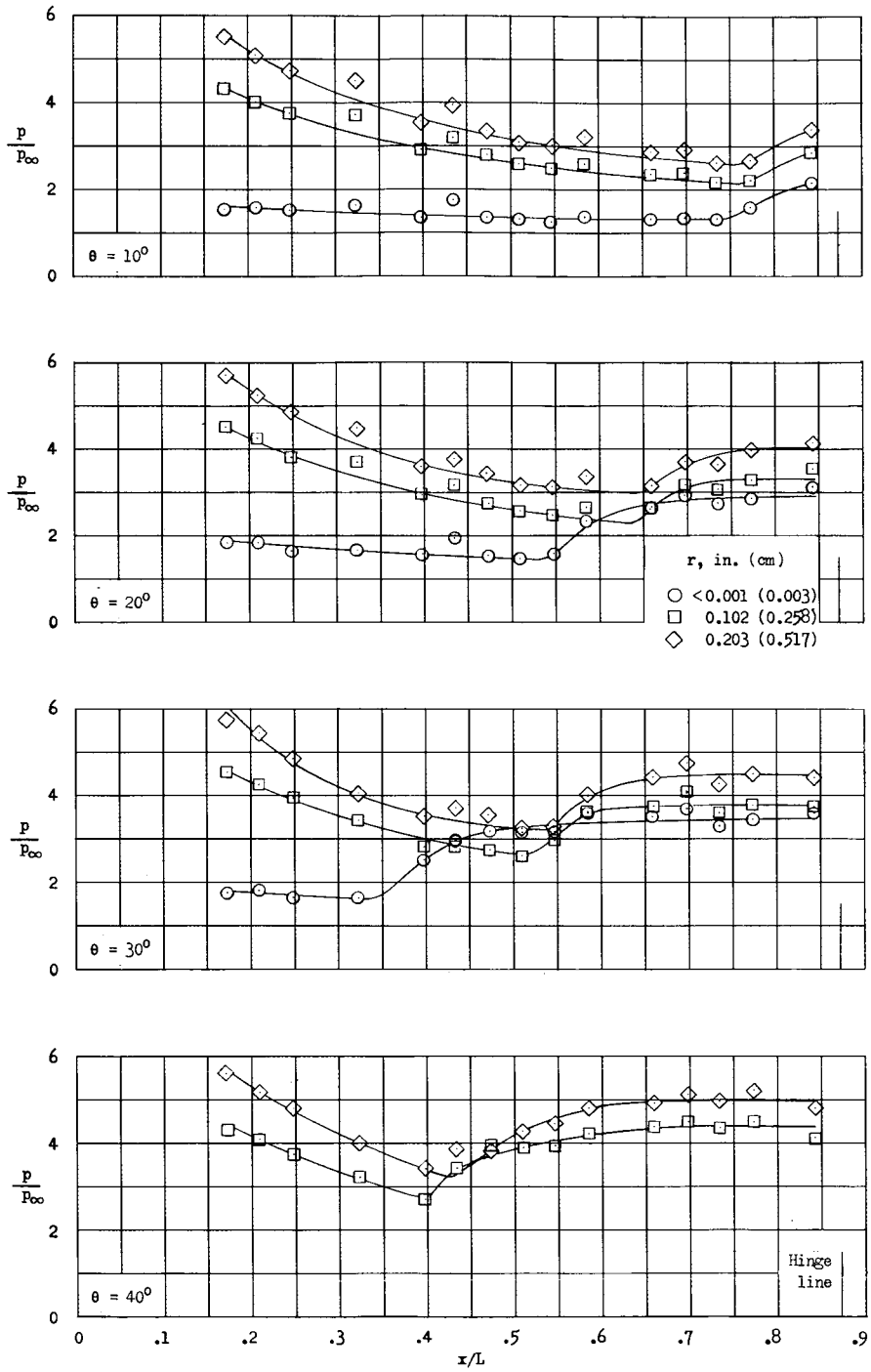

Figure 8.- Effect of leading-edge bluntness on the flat-plate pressure distributions for four ramp deflection angles. End plates on; $R_\infty/x = 1.26 \times 10^5$ per inch $(4.96 \times 10^6$ per meter$)$.

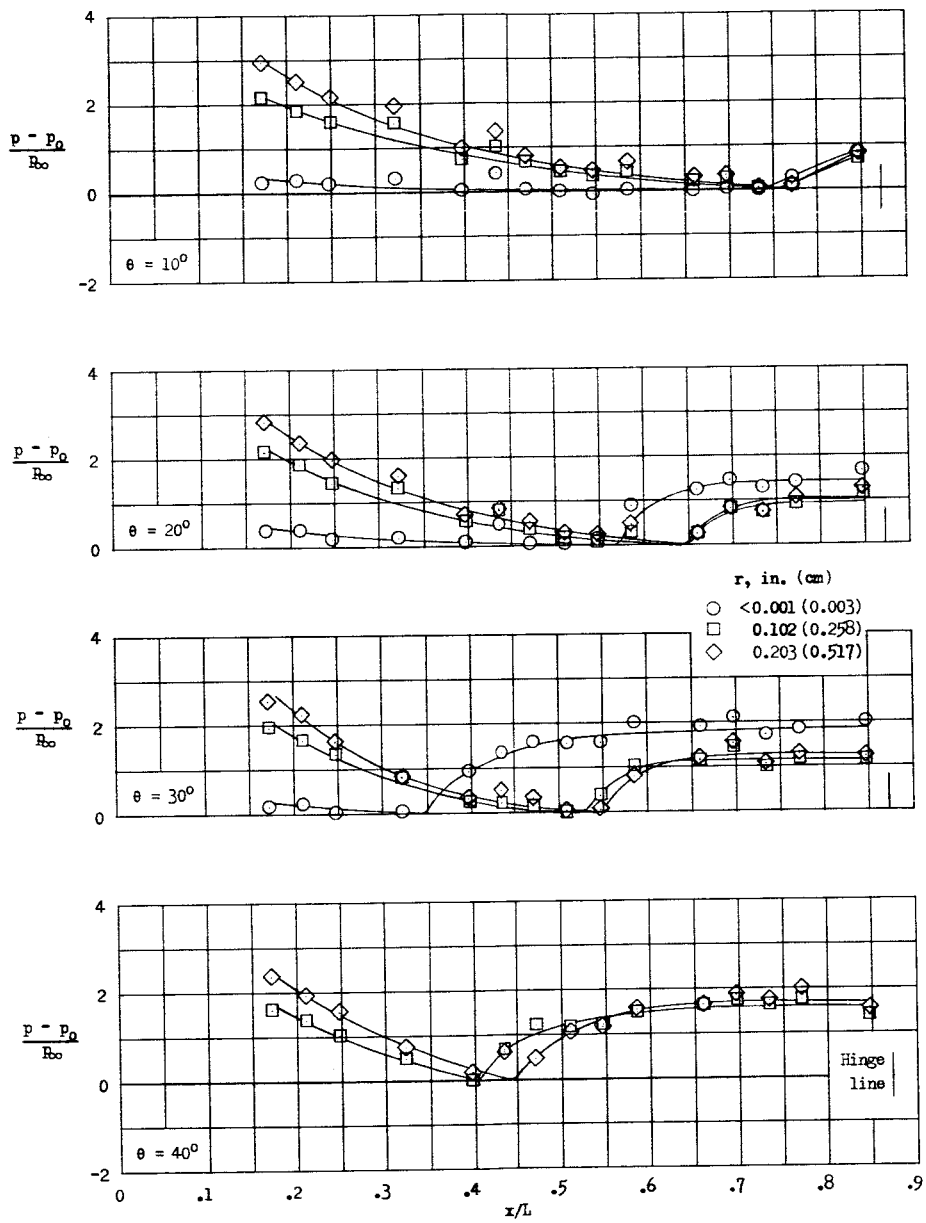

Figure 9.- Effect of leading-edge bluntness on the flat-plate pressure distributions based on the pressure at the beginning of the interaction for the four ramp angles. End plates on; $R_\infty/x = 1.26 \times 10^5$ per inch $(4.96 \times 10^6$ per meter).

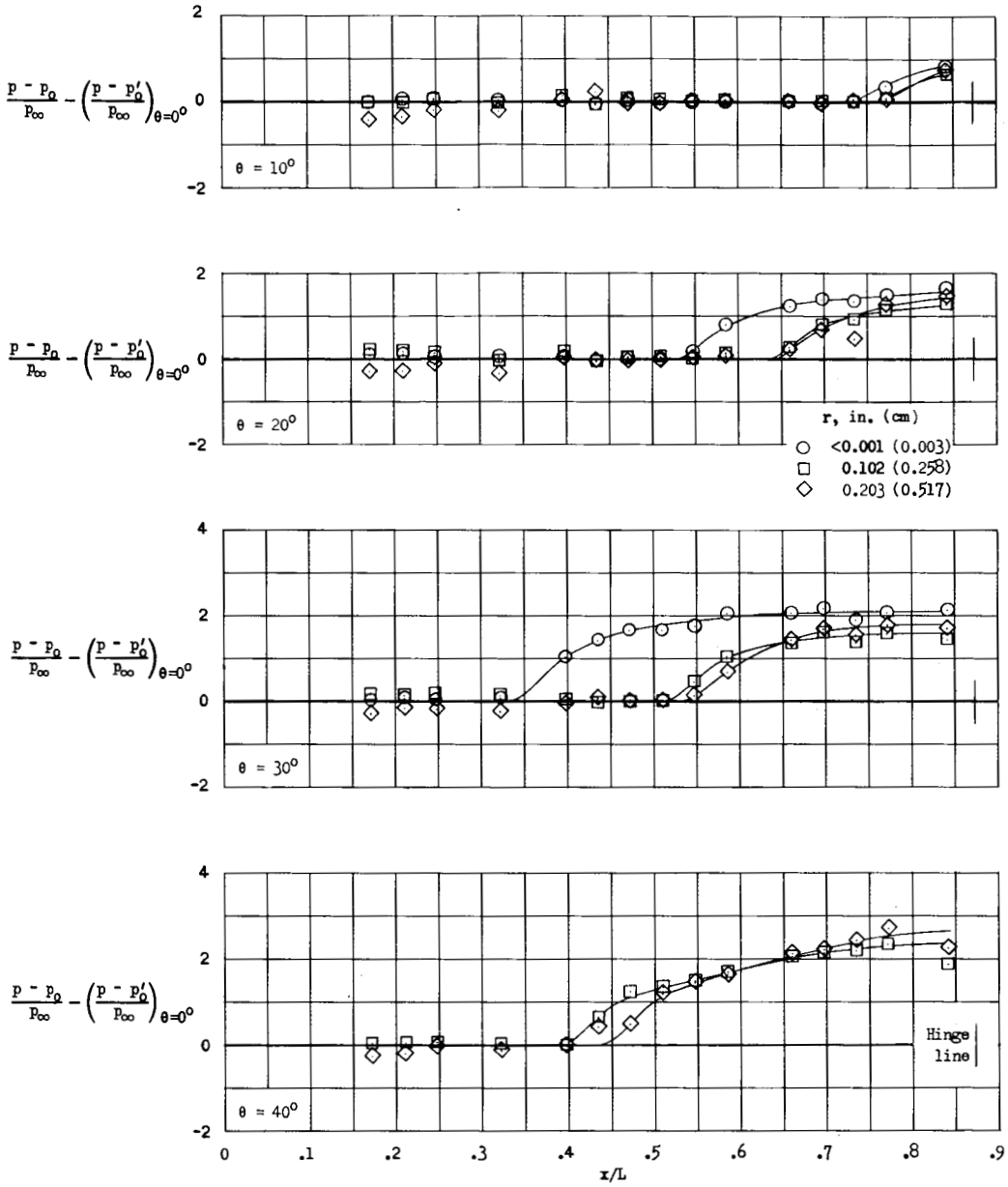

Figure 10.- Effect of leading-edge bluntness on the increase of the surface pressures above the flat-plate values for four ramp deflections. End plates on; $R_\infty/x = 1.26 \times 10^5$ per inch $(4.96 \times 10^6$ per meter).

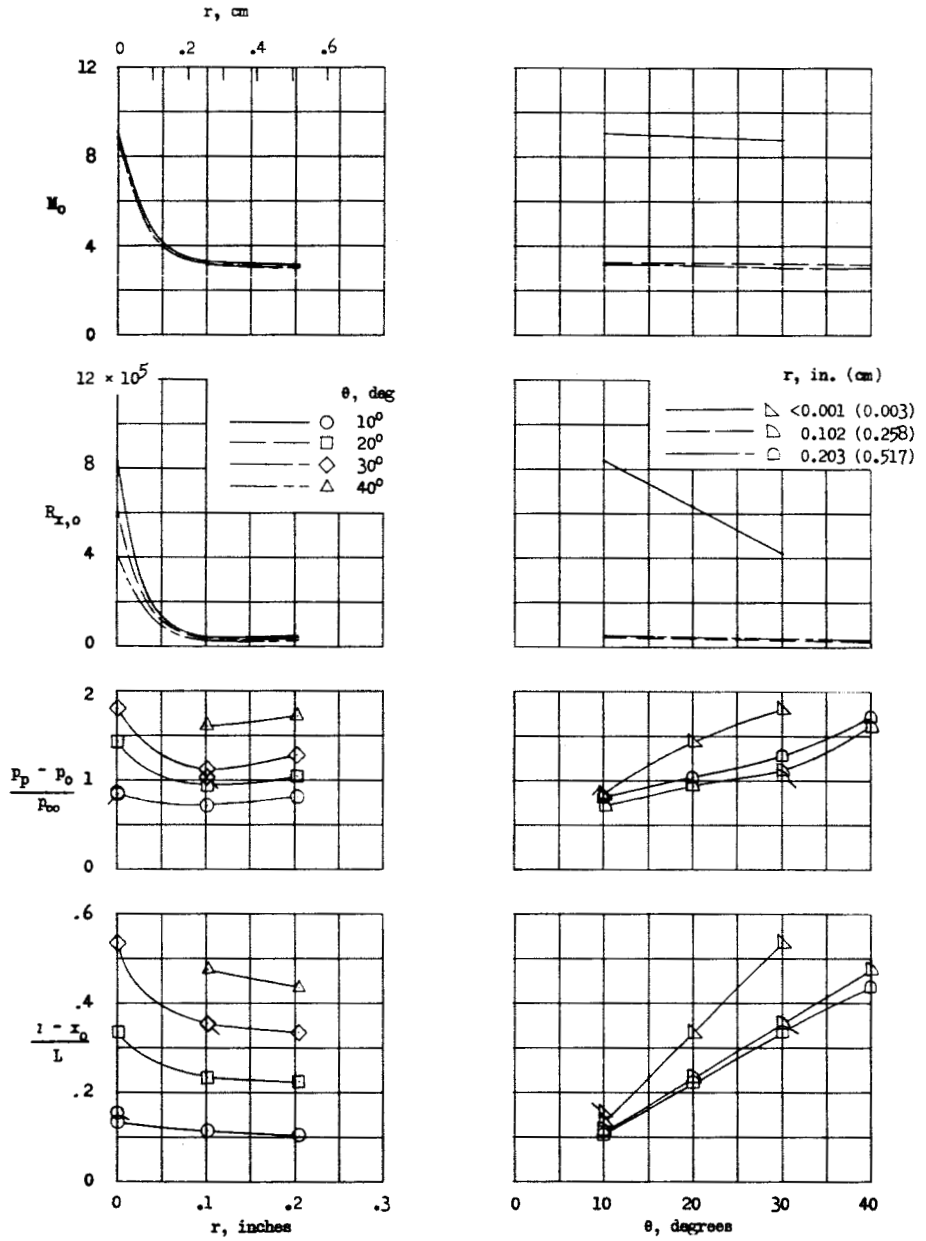

Figure 11.- Summary of the effects of leading-edge bluntness and ramp deflection angle on the plateau pressure and length of separated-flow region and on the local flow conditions at the beginning of the interaction leading to separation. End plates on; plain symbols indicate $R_\infty/x = 1.26 \times 10^5$ per inch $(4.96 \times 10^6$ per meter); flagged symbols indicate $R_\infty/x = 1.55 \times 10^5$ per inch $(6.10 \times 10^6$ per meter).

The results of reference 10 indicate that lowering the Mach number tends to reduce the plateau-pressure level and the extent of the separation region, whereas lowering the Reynolds number has the opposite tendency. It is evident from figure 11 that the Mach number reduction is dominant in the present case, in that a net decrease of more than one-third in both the pressure rise through interaction and the length from the beginning of the interaction to the ramp hinge line resulted from blunting the nose of the plate with the 30° ramp. Smaller decreases occurred for the 10° and 20° ramps. Another indication of the relative independence of the flow with respect to Reynolds number is shown by the flagged symbols. Reynolds number effects on laminar separation, of course, may be more important outside the ranges of Mach number and Reynolds number investigated.

Although the low Reynolds numbers on the blunt plates would appear to preclude it, there is a possibility of boundary-layer transition at reattachment due to the adverse pressure gradient in that region of the ramp. Even if transition should occur at reattachment, however, it is expected that the upstream effect of the transition on the separated region would be small and would consist mainly of a slight decrease in the plateau-pressure level. (For example, see figs. 11 and 12 of ref. 1.) The increased stability of laminar flow at high Mach numbers makes the occurrence of transition in the reattachment region on the sharp-leading-edge plates very unlikely. Inasmuch as reattachment of the separated boundary layer occurs toward the ends of the ramps and the effect of ramp length was not investigated, there is a possibility that longer ramps might allow larger separated regions to form in some instances and thus might affect the results regarding the length of the separated-flow region.

Comparison With Theory

Viscous-interaction theory.- The pressure distribution induced on a sharp-edge flat plate is a result of the displacement effect of the plate boundary layer on the external flow. Several theoretical methods for predicting the induced pressure distribution on a sharp-edge plate have been derived from analytical studies of the interaction phenomenon. The predictions of the first- and second-order weak interaction theories of reference 11 and the first-order strong interaction theory (for Prandtl number of 0.725) of reference 12 are compared with the present flat-plate pressure measurements (with $\theta = 0^{\circ}$) in figure 12. The modified second-order weak interaction theory of reference 12 was also calculated, but was found to coincide with the ordinary second-order theory of reference 11 for values of x/L greater than about 0.15 for the present test conditions. All three viscous-interaction predictions agree closely with one another and with the experimental results for the sharp-edge plate; thus the experimental accuracy does not justify selection of one theory from among them.

Blast-wave theory.- For a blunt-nose body the strong bow shock wave, rather than the viscous boundary layer, is the dominant influence in determining the flow. Thus, the pressure distribution on the blunt plate may be predicted by using two-dimensional blast-wave theory, which is based on an analogy to the unsteady flow resulting from a planar explosion. (See, for example, ref. 13.)

The predicted pressure distribution of blast-wave theory is compared in figure 12 with the experimental results of the present investigation. In general, the theoretical predictions are in good agreement with the measured pressure distributions on the flat plate ($\theta = 0^{\circ}$) for the two blunt noses.

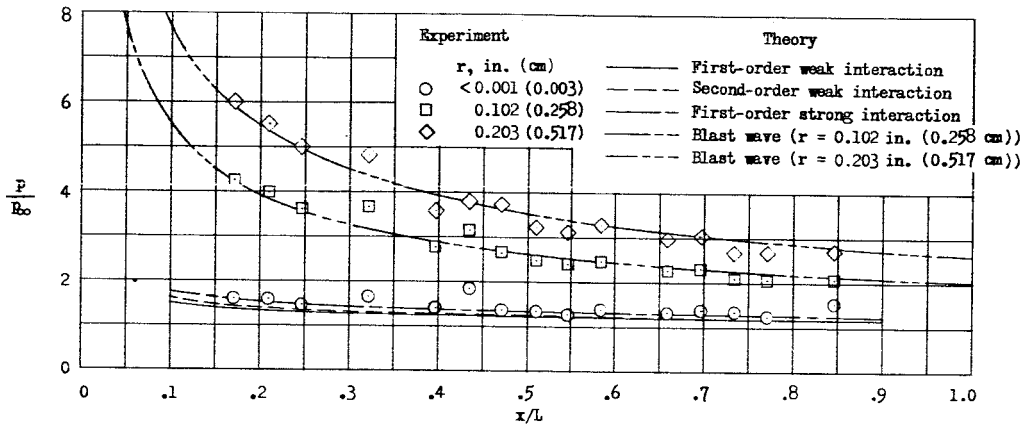

Figure 12.- Effect of leading-edge bluntness on the flat-plate pressure distribution with no ramp deflection ($\theta = 0^{\circ}$). End plates on; $R_{\infty}/x = 1.26 \times 10^{5}$ per inch $(4.96 \times 10^{6}$ per meter).

Correlation of plateau pressure coefficients.- As was shown in figures 11 and 12, the strong shock wave generated by a blunt nose produces flow conditions near the plate surface which are quite different from those encountered at the corresponding point on the sharp-nose plate. The investigations reported in references 1 and 14 and other sources have indicated that separation phenomena are strongly dependent on the local flow conditions at the beginning of the interaction leading to separation. Therefore, any comparison of separated flows influenced by various leading-edge bluntnesses probably should be based on these local conditions. Order-of-magnitude studies reported in reference 1 have shown that the plateau pressure rise may be expected to follow the relation $C_{p,p} = K\beta_{o}^{-1/2}R_{x,o}^{-1/4}$, the empirical value of K obtained from the experimental data of reference 1 being 1.82. Similar relations have been obtained in references 2 and 15 with values of K on the order of 1.90. An expression for the pressure distribution in the separated-flow region was developed in reference 14 by using certain empirical, universal functions; the plateau pressure rise was predicted as $C_{p,p} = 1.47\sqrt{\frac{2c_{f,o}}{\beta_{o}}}$.

In figure 13, the plateau pressure-rise coefficients obtained from all the present tests (with end plates) are compared with the results of references 1, 2, 3, 4, and 9 for shock-induced flow separation on sharp-leading-edge flat plates. Also presented in the figure are the correlation curves of references 1 and 14. As indicated in figure 11, the data from the present tests are seen to divide into two groups: the sharp-nose results ($r < 0.001$ inch (0.003 cm)) near $M_{o} = 9$, and the blunt-nose results ($r = 0.102$ and 0.203 inch (0.258 and 0.517 cm)) near $M_{o} = 3$. It should be noted that the two lowest points in each

group are data from the 10° ramp configurations, for which the plateau pressure is not well defined by the present measurements.

The plateau pressure-rise coefficients for the sharp-leading-edge plates with ramps deflected 20° and 30° ($M \approx 9$) are seen in figure 13(a) to agree fairly well with results obtained on similar configurations. The differences are partly if not wholly due to different assumptions for the leading-edge shock strength. However, except for $\theta = 40°$, the data for the blunt-nose plates ($M \approx 3$) are seen to fall somewhat below the semiempirical curves, an indication that the use of the local Mach number and Reynolds number is not completely adequate for correlation of data from both blunt- and sharp-leading-edge configurations. A possible reason for this inadequacy is the difference between the pressure distributions of the blunt plates (large favorable pressure gradients) and the sharp plates (small or zero pressure gradients). The boundary-layer momentum, which is strongly influenced by the pressure history, is fundamentally involved in the separation process, and thus the differences in pressure distribution may be expected to have significant effects on the characteristics of the separated-flow region.

In order to investigate the effects of pressure-distribution differences, the boundary-layer momentum thickness on the blunt plates was calculated by using the similar solutions for compressible laminar boundary layers from reference 16, applied in a manner similar to that suggested in reference 17. The

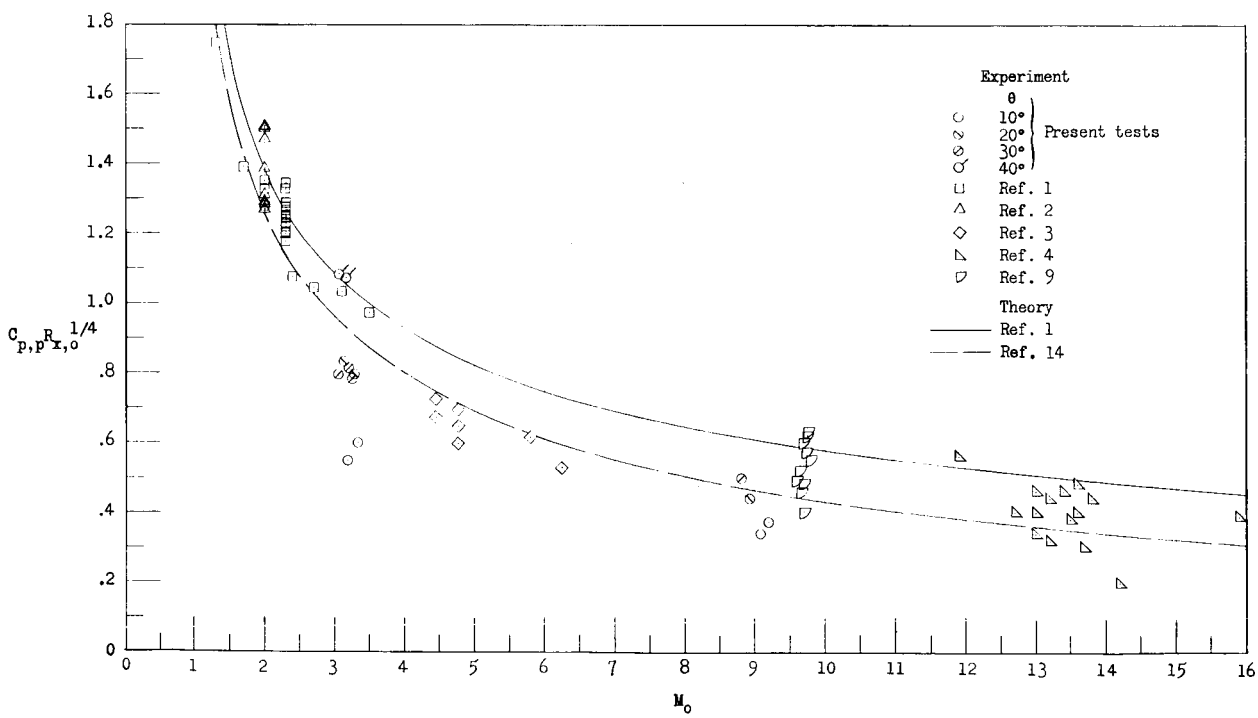

(a) Reynolds number based on x_o.

Figure 13.- Correlation of the plateau pressure coefficient on the basis of the local flow conditions at the beginning of the interaction. End plates on.

inviscid surface pressure distribution (and hence the velocity distribution, if isentropic flow behind the shock wave is assumed) was computed by modified Newtonian theory in the nose region up to the point where the pressure equaled that predicted by blast-wave theory and was computed by blast-wave theory (shown in fig. 12) beyond this point. With the variables converted to incompressible form by a Stewartson transformation (ref. 16), the velocity distribution was graphically approximated by two power laws chosen to match the momentum thickness at the juncture. The heat transfer in each of the two parts was assumed constant, and the momentum-thickness distribution was found for the chosen velocity power laws by using the similar solutions of reference 16. For comparison with the sharp-leading-edge results, a further calculation was made to find the length of a zero-pressure-gradient flat plate $\bar{x}_o$ necessary to produce the calculated momentum thickness at the beginning of the interaction on the blunt plates. The results shown in figure 13(b) were obtained by replacing x_o with $\bar{x}_o$ in the Reynolds number for the blunt plates. The data points in figure 13(b) for the blunt-nose plates ($M_o \approx 3$) are seen to be higher than the corresponding data points in figure 13(a); therefore, for the 20° and 30° ramp deflections, there is very good agreement with the empirical correlation curves based on sharp-leading-edge data. For $\theta = 40^\circ$, however, the values obtained are higher than the correlation curve, possibly because at this high deflection angle the shock at reattachment is detached from the ramp.

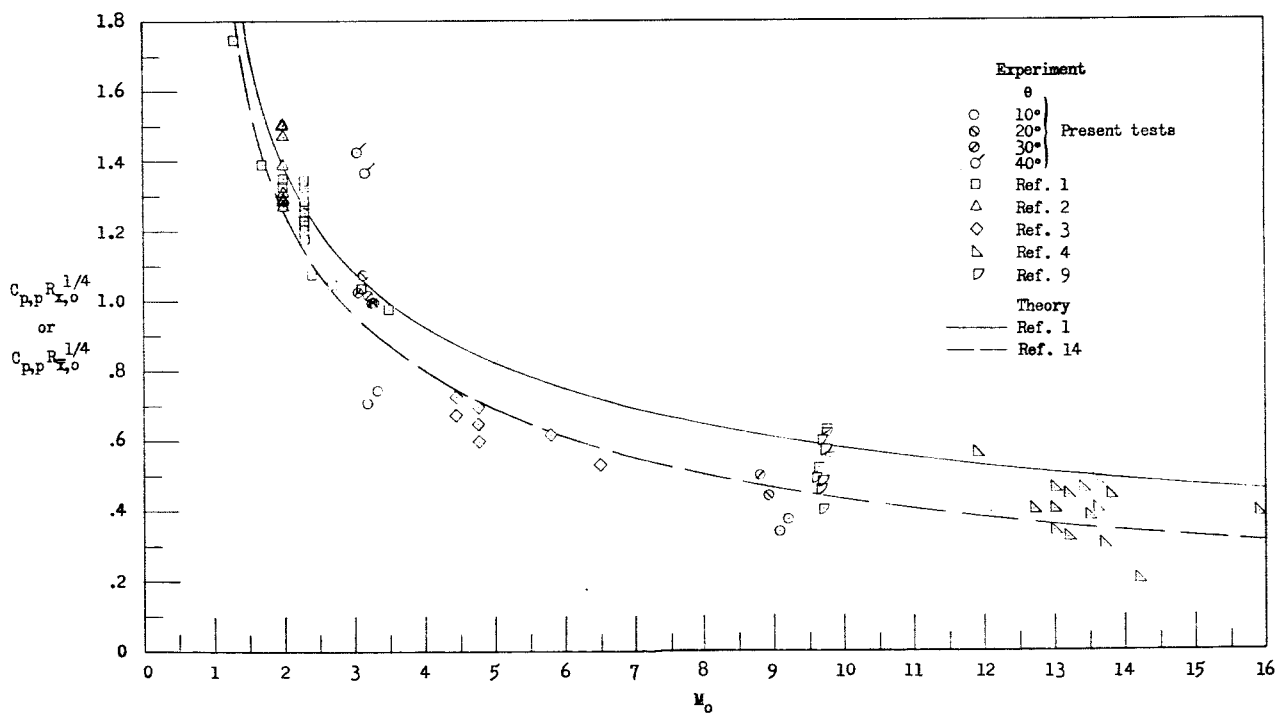

(b) Reynolds number for sharp plates based on x_o, for blunted plates on the length on a sharp plate for the equivalent boundary-layer momentum-thickness development $\bar{x}_o$.

Figure 13.- Concluded.

The improvement in the correlation obtained in figure 13(b) over that of figure 13(a) shows that the boundary-layer momentum is important in determining the separation characteristics of laminar boundary layers. These results indicate that the boundary-layer momentum thickness, in conjunction with the local Mach number and Reynolds number at the beginning of the interaction, forms the proper basis for comparison of boundary-layer separation on sharp- and blunt-leading-edge configurations in hypersonic flow. These same parameters are expected to be useful in the analysis of the effects of other flow disturbances ahead of separated-flow regions.

CONCLUSIONS

An investigation has been conducted in the Langley 15-inch hypersonic flow apparatus to determine the effects of leading-edge bluntness on the characteristics of laminar boundary-layer separation ahead of ramps on a flat plate. The tests were made at a Mach number of 10.03 and nominal Reynolds numbers of 1.26×10^5 and 1.56×10^5 per inch (4.96×10^6 and 6.14×10^6 per meter), with the plate at zero angle of attack. End plates were used on the model to approximate two-dimensional flow conditions.

The results of the investigation indicate the following:

1. Within the ranges of variables in the present test series, leading-edge bluntness reduces the effects of laminar boundary-layer separation by decreasing both the length of the separated-flow region and the pressure rise through separation.

2. The decreases in separation pressure rise and in length of the separated-flow region ahead of a 30° ramp amount to more than one-third of the sharp-leading-edge values for an increase in leading-edge radius from less than 0.001 to 0.102 inch (radius less than 0.003 to 0.258 cm), with smaller reductions occurring at smaller ramp angles.

3. Only a small additional reduction in the length of separation and practically no further reduction in the pressure rise occur as the nose radius is increased from 0.102 to 0.203 inch (0.258 to 0.517 cm).

4. Correlation of blunt-nose data with those from sharp-leading-edge plates shows that the boundary-layer momentum thickness and the local Mach number and Reynolds number at the beginning of the interaction form the proper basis for comparison of boundary-layer separation characteristics on blunt- and sharp-nose configurations.

Langley Research Center,
National Aeronautics and Space Administration,
Langley Station, Hampton, Va., November 10, 1965.

REFERENCES

1. Chapman, Dean R.; Kuehn, Donald M.; and Larson, Howard K.: Investigation of Separated Flows in Supersonic and Subsonic Streams With Emphasis on the Effect of Transition. NACA Rept. 1356, 1958. (Supersedes NACA TN 3869.)

2. Hakkinen, R. J.; Greber, I.; Trilling, L.; and Abarbanel, S. S.: The Interaction of an Oblique Shock Wave With a Laminar Boundary Layer. NASA MEMO 2-18-59W, 1959.

3. Sterrett, James R.; and Emery, James C.: Extension of Boundary-Layer-Separation Criteria to a Mach Number of 6.5 by Utilizing Flat Plates With Forward-Facing Steps. NASA TN D-618, 1960.

4. Miller, D. S.; Hijman, R.; and Childs, M. E.: Mach 8 to 22 Studies of Flow Separations Due to Deflected Control Surfaces. AIAA J., vol. 2, no. 2, Feb. 1964, pp. 312-321.

5. Mechtly, E. A.: The International System of Units - Physical Constants and Conversion Factors. NASA SP-7012, 1964.

6. Putnam, Lawrence E.; and Brooks, Cuyler W., Jr.: Static Longitudinal Aerodynamic Characteristics at a Mach Number of 10.03 of Low-Aspect-Ratio Wing-Body Configurations Suitable for Reentry. NASA TM X-733, 1962.

7. Daum, Fred L.: Air Condensation in a Hypersonic Wind Tunnel. AIAA J., vol. 1, no. 5, May 1963, pp. 1043-1046.

8. Goranson, George G.; Jaffe, Peter; Steuer, Guenter; and Dayman, Bain, Jr.: Additional Observations of the Effects of Air Condensation in the 21-Inch Hypersonic Wind Tunnel. Tech. Release No. 34-153 (Contract NASw-6), Jet Propulsion Lab., C.I.T., Oct. 26, 1960.

9. Putnam, Lawrence E.: Investigation of Effects of Ramp Span and Deflection Angle on Laminar Boundary-Layer Separation at Mach 10.03. NASA TN D-2833, 1965.

10. Gray, J. Don: A Correlation of Axisymmetric Laminar Flow Separation Characteristics. Paper No. 64-475, Am. Inst. Aeron, Astronaut., July 1964.

11. Lees, Lester; and Probstein, Ronald F.: Hypersonic Viscous Flow Over a Flat Plate. Rept. No. 195 (Contract AF 33(038)-250), Aeron. Eng. Lab., Princeton Univ., Apr. 20, 1952.

12. Bertram, Mitchel H.; and Blackstock, Thomas A.: Some Simple Solutions to the Problem of Predicting Boundary-Layer Self-Induced Pressures. NASA TN D-798, 1961.

13. Chernyi, G. G. (Ronald F. Probstein, trans.): Introduction to Hypersonic Flow. Academic Press, Inc., 1961.

14. Erdos, John; and Pallone, Adrian: Shock-Boundary Layer Interaction and Flow Separation. RAD-TR-61-23, Res. and Advanced Develop. Div., AVCO Corp., Aug. 15, 1961.

15. Gadd, G. E.: A Theoretical Investigation of Laminar Separation in Supersonic Flow. J. Aeron. Sci., vol. 24, no. 10, Oct. 1957, pp. 759-771.

16. Cohen, Clarence B.; and Reshotko, Eli: Similar Solutions for the Compressible Laminar Boundary Layer With Heat Transfer and Pressure Gradient. NACA Rept. 1293, 1956. (Supersedes NACA TN 3325.)

17. Smith, A. M. O.: Rapid Laminar Boundary-Layer Calculations by Piecewise Application of Similar Solutions. J. Aeron. Sci., vol. 23, no. 10, Oct. 1956, pp. 901-912.

NASA-Langley, 1966 L-4207